

Nonclassical Light Generation in Two-Emitter-Cavity Systems

Marina Radulaski,* Kevin A. Fischer, Konstantinos G. Lagoudakis, Jingyuan Linda Zhang, and Jelena Vučković
E. L. Ginzton Laboratory, Stanford University, Stanford, California 94305, United States
(Dated: May 6, 2022)

We study n -photon generation in multi-emitter cavity systems with small inhomogeneous broadening, characteristic of color center systems. We focus on the case of $N = 2$ nonidentical quasi-atoms strongly coupled to a nanoresonator in the bad cavity regime. Using the quantum master equation in an extended Tavis-Cummings model, we discover a new interference effect resulting in high quality single-photon generation that is robust to emitter property variations. We also identify conditions of conventional and un-conventional photon blockade, which promote $n = 1$ and $n = 3$ photon generation, respectively. We explain the origin of these phenomena via the effective Hamiltonian approach.

Introduction—Cavity quantum electrodynamics (CQED) studies phenomena, such as photon blockade and photon-induced tunneling, that produce nonclassical light in the form of n -photon emission. Applications of n -photon bundles are wide ranging and include quantum key distribution [1], quantum metrology [2] and quantum computation [3]. While CQED systems have been extensively studied in atomic platforms [4, 5], a significant advance in terms of operating rates and on-chip integration took place with their subsequent implementation in the solid-state. Notably, the InAs/GaAs quantum dot platform has been used to develop devices with GHz speeds, such as the single-photon source [6, 7] and the low-power all-optical switch [8–10]. The ability to use multiple ($N > 1$) nearly-identical emitters, as opposed to one, would further increase the interaction rate by a factor of \sqrt{N} via the effects of collective coupling [11, 12]. This would in turn provide higher speed and quality of on-chip CQED devices. However, the large inhomogeneous broadening among quantum dots is prohibitive of this advance.

Recently, a solid-state CQED platform with smaller inhomogeneous broadening—rare-earth ions in a nanocavity—achieved the strong multi-emitter cavity coupling using a large ($N \sim 10^6$) ensemble of emitters [13]. In this limit, however, the rungs of the energy ladder approximate a continuum of modes, and are therefore not suitable for non-classical light generation. In contrast, coupling several ($N \gtrsim 1$) emitters to a cavity would preserve the desired discrete energy character, but would also require emitters to have larger dipole moments. Such values have been seen among color centers in diamond and silicon carbide incorporated into emitter-cavity platforms [14–17]. With inhomogeneous broadening often less than 30 GHz [18, 19] these quasi-atoms could meet the requirements for multi-emitter strong CQED coupling if hosted in high quality factor and small mode volume cavities. This regime has been studied for superconducting cavities [20] and is characterized by the collective emitter

coupling rate $G_N = \sqrt{\sum_{n=1}^N g_n^2}$ that is dominant over the cavity (κ) and emitter (γ) linewidth-induced loss mechanisms: $G_N > \kappa/2, \gamma/2$. Currently, little is known about coherence properties of such systems and their potential for nonclassical light generation.

We consider theoretically the coherence effects in a $N = 2$ multi-emitter CQED system [Fig. 1(a)] and analyze the influence of inhomogeneous broadening to n -photon generation. Using the quantum master equation in an extended Tavis-Cummings model, we discover a new interference effect resulting in high quality single-photon generation that is robust to emitter property variations. We also identify conditions of conventional and un-conventional photon blockade, which promote $n = 1$ and $n = 3$ photon generation, respectively. We explain the origin of these phenomena via the effective Hamiltonian approach.

The model—The interaction Hamiltonian for our CQED system consists of the cavity, emitter and coupling terms ($\hbar = 1$):

$$H_I = \omega_C a^\dagger a + \sum_{n=1}^N [\omega_{En} \sigma_n^\dagger \sigma_n + g_n (\sigma_n^\dagger a + a^\dagger \sigma_n)],$$

where a and ω_C represent the annihilation operator and resonant frequency of the cavity mode; σ_n , g_n and ω_{En} are the lowering operator, cavity coupling strength and transition frequency of the n -th out of $N = 2$ emitters.

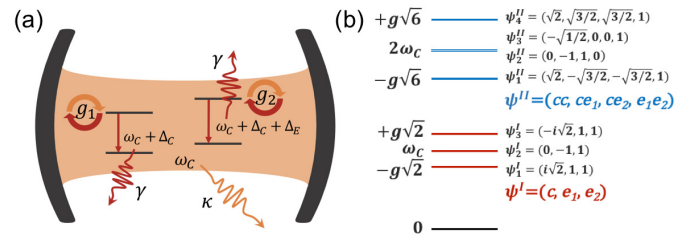


FIG. 1. (a) An illustration of the multi-emitter CQED system with two nonidentical emitters coupled to a common cavity mode. (b) The ladder of dressed states, frequencies and unnormalized eigenvectors, for the case of two identical and equally coupled emitters, $\Delta_C = \Delta_E = 0$ and $g_1 = g_2 = g$.

* marina.radulaski@stanford.edu

To treat the cavity and emitter detunings more explicitly, we rewrite emitter frequencies as $\omega_{E1} = \omega_C + \Delta_C$ and $\omega_{E2} = \omega_C + \Delta_C + \Delta_E$.

The system is characterized by the cavity energy decay and emitter linewidth $\{\kappa, \gamma\}/2\pi = \{25, 0.1\}$ GHz, corresponding to quality factor $Q \approx 15,000$, emitter lifetime $\tau = 10$ ns, and the individual emitter-cavity coupling rate $g_n/2\pi = 10$ GHz. Comparing to the state-of-the-art results with silicon-vacancy centers in a photonic crystal cavity [17], the quoted values could be achieved by designing nanocavities with doubled quality factor and five-fold increased coupling rate, which can be achieved by reducing the mode volume several times and providing higher-precision positioning of the color centers at the field maximum [21]. The three-fold mismatch in emitter linewidth, which is the smallest rate in the system, is tolerable in the bad cavity regime. With the imposed set of parameters, a single emitter would be weakly coupled to the cavity ($g_n < \kappa/2$), however, the collective coupling of two emitters would bring the system into the strong coupling regime ($\sqrt{g_1^2 + g_2^2} > \kappa/2$). The former condition is not required, however, it provides looser expectations toward the nanofabrication process.

To model the interaction of the system with its environment, we use the quantum master equation to calculate the steady state solution of the density matrix ρ :

$$\dot{\rho} = -i[H_I + E_P(ae^{i\omega t} + a^\dagger e^{-i\omega t}), \rho] + \kappa\mathcal{L}[a] + \sum_{n=1}^N \gamma\mathcal{L}[\sigma_n],$$

where $E_P = \kappa/50$ represents the laser field amplitude, and loss terms are introduced through the superoperator $\mathcal{L}[O] = O\rho(t)O^\dagger - \frac{1}{2}\rho(t)O^\dagger O - \frac{1}{2}O^\dagger O\rho(t)$. The system is then transformed into a rotating frame to remove the time-dependence [22] and obtain the steady state solution. When calculating emission spectra as $\langle a^\dagger a \rangle$, we leave the E_P term out and add a pump term in the Liouvillian as $P\mathcal{L}[a^\dagger]$, where P represent the laser power.

We gain a more intuitive understanding of the system dynamics by diagonalizing the effective Hamiltonian, constructed with the complex frequencies that account for cavity and emitter loss [20]:

$$H_{\text{eff}} = H_I - \frac{\kappa}{2}a^\dagger a - \sum_{n=1}^N \frac{\gamma}{2}\sigma_n^\dagger \sigma_n.$$

The real and the imaginary part of its eigenvalues represent frequencies and half-linewidths of the excited energy states, respectively, while the eigenvectors quantify the cavity-like and the emitter-like character of the excited state. Figure 1(b) shows the eigenfrequencies and eigenvectors in the ladder of dressed states for an identical and equally coupled system. The eigenvector elements are labeled with c for cavity, e_1 and e_2 for the first and the second emitter excitation, respectively. In contrast to CQED systems with a single emitter where all excited states contain two levels, here we see that an additional emitter generates new excited states. The new middle

state in the first rung resembles the wavefunction of a subradiant state $(e_2 - e_1)/\sqrt{2}$, known from atomic systems not to couple to the environment. There are also two new middle states in the second rung, which are degenerate for this set of detunings. These additional levels ultimately lead to a much richer set of physics phenomena. Not only do we find an enhanced regime of photon blockade from the subradiant states, but a newly discovered un-conventional photon blockade regime [23] can also be achieved in the system. We now explore these effects as a function of the emitter detuning Δ_E .

Results—We present calculation results for cavity detunings $\Delta_C/2\pi = 0, 20$ and 30 GHz which capture system's trends and features. The emission spectra are shown in Fig. 2(a). In parallel, we calculate the eigenstates of the first rung of the effective Hamiltonian, shown as red surfaces in Fig. 2(d). The three transmission peaks are in a close agreement with these eigenfrequencies, which expectedly indicates that the bottom peak is cavity-like, and the top two peaks emitter-like. To more closely understand the effects that non-identical emitters bring into CQED, we now focus on the emerging subradiant state for $\Delta_E/2\pi \leq 3$ GHz. Qualitatively similar spectra have been calculated for superconducting cavities coupled to an ensemble of spins [24] and experimentally observed in superconducting circuits [25]. The collective strong coupling rate $G_2 = \sqrt{g_1^2 + g_2^2}$ places the two polariton peak frequencies close to $\omega_{\text{pol}\pm}^{\Delta_E=0} = \omega_C + \frac{\Delta_C}{2} - i\frac{\kappa+\gamma}{4} \pm \frac{\sqrt{4\Delta_C^2 + 16G_2^2 + 2\kappa\gamma + 4i\Delta_C\kappa - 4i\Delta_C\gamma + i\kappa^2 + i\gamma^2}}{4}$. Here, we describe the subradiant state in more detail by deriving approximations to its frequency ω_{sub} and state vector v_{sub} for $\Delta_E \ll G_2, \frac{\kappa-\gamma}{2}$:

$$\omega_{\text{sub}} = \omega_C + \Delta_C + \frac{g_1^2}{G_2^2} \Delta_E - i \left(\frac{\gamma}{2} + \frac{\kappa - \gamma}{8G_2^2} \Delta_E^2 \right),$$

$$v_{\text{sub}} = \frac{1}{\sqrt{A}} \begin{bmatrix} -\frac{g_2 \Delta_E}{G_2^2} + i \frac{\kappa - \gamma}{8g_2} \frac{\Delta_E^2}{G_2^2} \\ -\frac{g_1}{g_2} \frac{8g_2^2 + i(\kappa - \gamma)\Delta_E}{8g_1^2 - i(\kappa - \gamma)\Delta_E} \\ 1 \end{bmatrix},$$

where A is a normalization factor. For vanishing Δ_E the cavity term in v_{sub} becomes zero, diminishing state's coupling to the environment. With an increasing Δ_E , the frequency of the subradiant state grows linearly, while the linewidth and the amplitude increase quadratically, closely matching the trend in the simulated emission spectra for $\Delta_E/2\pi \leq 3$ GHz.

Next, we quantify the system's potential for n -photon generation by analyzing the second- and third-order coherence of light transmitted through the system [Figs. 2(b-c)]. Areas of suppressed $g^{(2)}(0)$ statistics (red areas) indicate the potential for single-photon emission, which is further supported if the $g^{(3)}(0)$ values are simultaneously reduced. We find such areas close the frequencies of the emission peaks, especially for higher detuned emitter-like peaks. This is consistent with the findings in

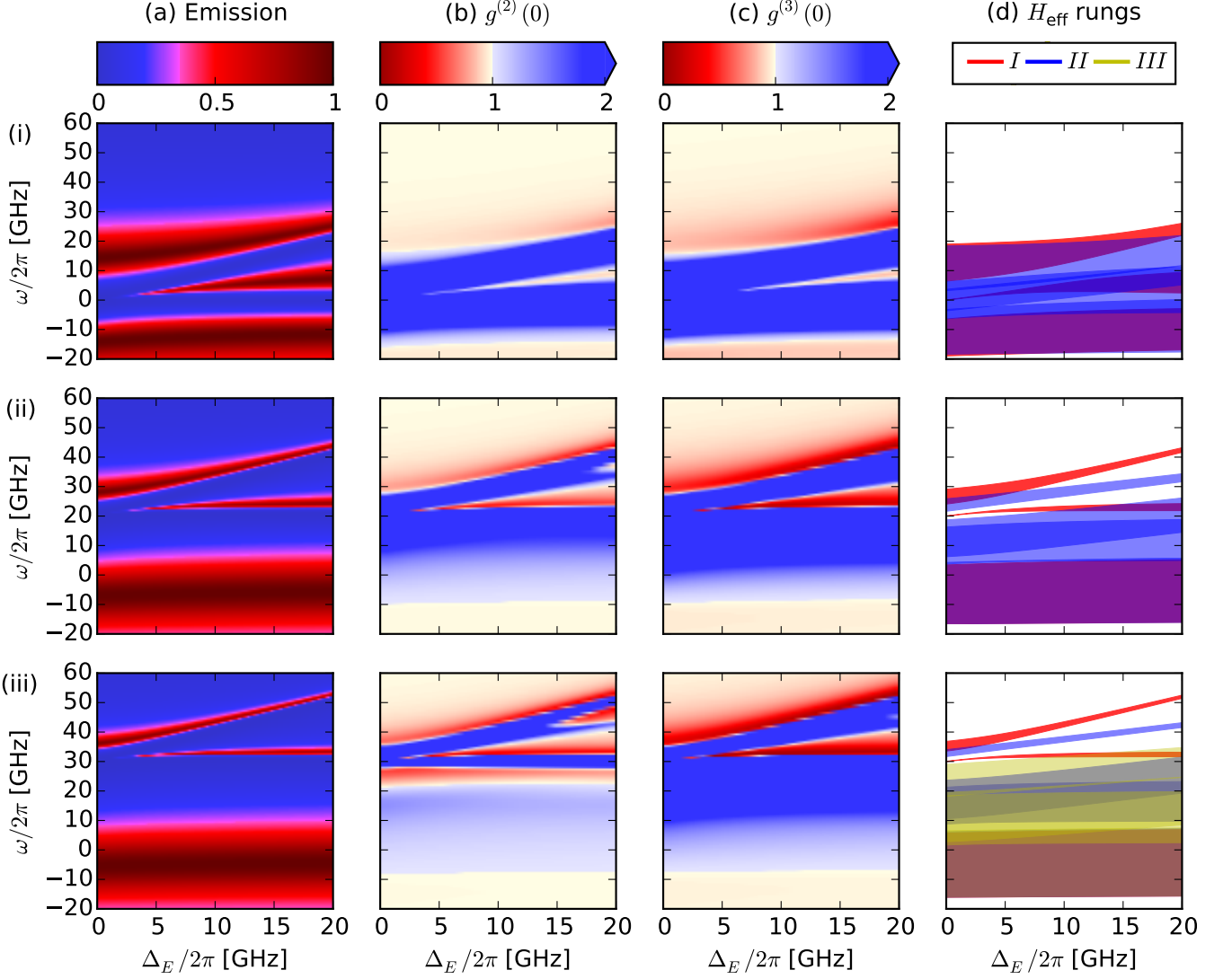


FIG. 2. (a) Emission spectrum, (b) second- and (c) third-order coherence of transmitted light calculated by the quantum master equation. (d) Frequency overlap between the k -th order rungs of the dressed ladder of states of H_{eff} , presented as $\omega_k/k - \omega_C$ with indicated linewidths; $\Delta_C/2\pi$ takes values of (i) 0, (ii) 20 and (iii) 30 GHz.

single-emitter CQED systems where the photon blockade at polariton peak frequency improves with emitter-cavity detuning [6]. However, there is no direct analog for the transmission through the newly formed subradiant state. We reveal the origin of both effects by analyzing the frequency overlap $E_k/k - \omega_C$ between eigenstates of different order (k) rungs of H_{eff} [Fig. 2(d)]. We find that the two photon emission is suppressed for the frequencies where single photon absorption is possible (red areas), but the second photon would not have a spectrally close state to be absorbed at (no overlapping blue areas). Surprisingly, for large Δ_E this condition disappears for the subradiant peak, but the photon blockade still persists. To understand this apparent contradiction, we perform an additional analysis of the eigenstate character for $\Delta_C/2\pi = 20$ GHz, presented in

Fig. 3. We find that for an increasing Δ_E the eigenstates $\psi_1^I, \psi_2^I, \psi_3^I, \psi_1^{II}, \psi_2^{II}, \psi_3^{II}$ and ψ_4^{II} (see Fig. [?]b), prevalently exhibit $c, e_1, e_2, cc, ce_1, ce_2$, and e_1e_2 character, respectively. Therefore, the dipolar coupling between ψ_2^I and ψ_3^{II} has to be inhibited due to $\langle ce_2 | a^\dagger | e_1 \rangle = 0$, which in turn suppresses the second photon absorption at the higher detunings. With this combination of spectral and vector component properties obtained from the diagonalization of the effective Hamiltonian we predict parameters that give rise to enhanced single photon emission. The properties also hold for nonidentically coupled emitters ($g_1 \neq g_2, G_2 > \kappa/2$), which has favorable practical implications for systems with randomly positioned color centers whose coupling strength can not be imposed uniformly.

In addition to these trends, we also find conditions

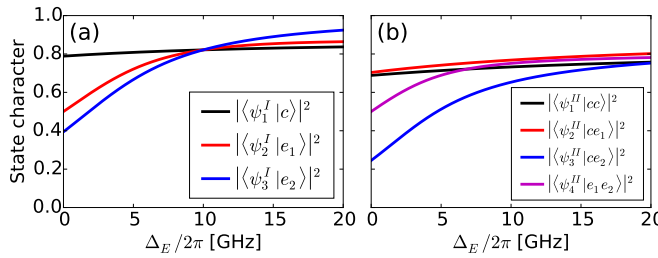


FIG. 3. Prevalent character of the eigenstates of (a) the first and (b) the second rung of H_{eff} for $\Delta_C = 20$ GHz.

for realization of a superbunching effect recently dubbed *unconventional photon blockade* [23], which confirms that the reduction in two-photon statistics is not a sufficient condition for single-photon emission. This effect occurs in the system with $\Delta_C/2\pi = 30$ GHz in the region around $\omega/2\pi = 25$ GHz which has a low $g^{(2)}(0)$ but high $g^{(3)}(0)$ value, indicating preferential three-photon emission. To understand the occurrence of this regime in our system, we look into the third rung of the dressed ladder shown in yellow at Fig. 2(d-iii) and reveal that this frequency region has an overlapping three-photon absorbing state, but no two-photon absorbing state, which explains the calculated statistics. Thus the multi-emitter CQED system will not just advance the single-photon blockade, but also allow for the exploration of exciting regimes of multiphoton physics and statistics.

Finally, we analyze the system dynamics in the time domain in terms of interferences between the excited states. We look into the three $g^{(2)}(0)$ dips for $\{\Delta_C, \Delta_E\}/2\pi = \{30, 5\}$ GHz [Fig. 4(a)]. The second-order coherence evolution at the frequency of the unconventional photon blockade [blue line in Fig. 4(b)] represents a damped oscillation and once again confirms that the system can not be a good single photon source at these frequencies. The dominant oscillation frequency ($\omega/2\pi$) is 5.2 GHz, while the first 200 ps also exhibit additional 11 GHz oscillation. The other two second-order coherence traces are at frequencies of conventional photon blockade, and represent a decay to a coherent state. The characteristic half-width at half-maximum times are 0.7 ns and 0.2 ns for the transmission through states with e_1 (yellow) and e_2 (green) characters, respectively, and represent a speedup in single photon emission compared to a bare quasi-emitter. Both functions exhibit 44 GHz oscillations with small amplitudes in the first 200 ps, which corresponds to the oscillation between the polaritonic eigenstates of the first rung of the dressed ladder and is analogous to the experimentally observed oscillations in single atom-cavity systems [26]. The function plotted in green also oscillates at 7.7 GHz at longer times, whose origin we assign to the interference between the upper polaritonic and the subradiant states. We observe this trend for other sets of parameters as well.

Discussion—Comparing nonclassical light generation

in our $N = 2$ multi-emitter-cavity system with $N = 1$ case [6], we both predict lower values of $g^{(2)}(0)$ —even when compared to a single-emitter system with coupling rate of $g\sqrt{2}$ —and find opportunities for more robust single photon generation. The frequency and the second-order coherence values of light transmitted through the state ψ_2^I are close to constant for variable emitter detuning. Practically, this implies that for any pair of nonidentical emitters (3 GHz $\leq \Delta_E/2\pi \leq 20$ GHz) the quality of single photon emission is dictated by the cavity detuning from the first emitter. Experimentally, the cavity detuning can be controlled by gas tuning techniques without influencing the operating laser frequency [17].

In conclusion, we have analyzed nonclassical light generation in a strongly coupled two-emitter CQED system for variable cavity and emitter detuning. Combining quantum master equation and effective Hamiltonian approaches, we identified the parameters that give rise to robust photon blockade, and explained their origin in the overlap between the eigenstates of multiple rungs of the dressed ladder. We also characterized the oscillations in $g^{(2)}(\tau)$ function as interference between the states of the first rung. The time scale of the single photon emission represents an order of magnitude speedup over the bare emitter dynamics, while the $g^{(2)}(0)$ values are improved over the system with a single emitter in a cavity. In light of the presented opportunities in conventional and un-conventional photon blockade, multi-photon emission and operating rate speedup, we expect that $N > 2$ multi-emitter CQED systems will unveil even richer physics. For systems with more than several emitters, numerical calculations may prove lengthy due to the large size of the density matrix, however, our theoretical analysis based on the diagonalization of the effective Hamiltonian can provide a quick insight into the potential parameter areas with robust single photon emission.

Acknowledgements—This work has been supported by the National Science Foundation (DMR Grant Numbers 1406028 and 1503759). We thank Hideo Mabuchi, Nikolas Tezak and Dmitri Pavlichin for constructive discussions. K.A.F. acknowledges support from the Lu Stanford Graduate Fellowship and the National Defense Science and Engineering Graduate Fellowship.

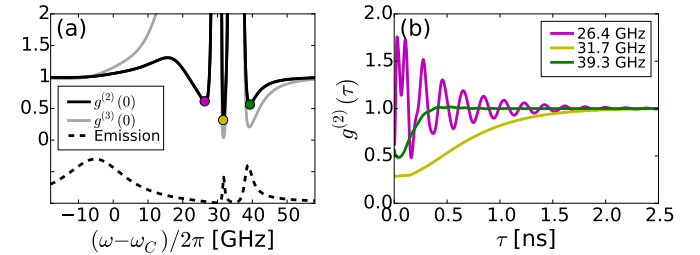


FIG. 4. (a) Zero-delay second- and third-order coherences for $\Delta_C, \Delta_E/2\pi = 30, 5$ GHz system as a function of laser detuning from the cavity; emission spectrum in dashed lines illustrates the relationship between features. (b) $g^{(2)}(\tau)$ at frequencies of the corresponding $g^{(2)}(0)$ minima from (a).

[1] J. L. O'Brien, A. Furusawa, and J. Vučković, *Nature Photonics* **3**, 687 (2009).

[2] V. Giovannetti, S. Lloyd, and L. Maccone, *Physical review letters* **96**, 010401 (2006).

[3] E. Knill, R. Laflamme, and G. J. Milburn, *nature* **409**, 46 (2001).

[4] S. Haroche and D. Kleppner, *Phys. Today* **42**, 24 (1989).

[5] K. M. Birnbaum, A. Boca, R. Miller, A. D. Boozer, T. E. Northup, and H. J. Kimble, *Nature* **436**, 87 (2005).

[6] K. Müller, A. Rundquist, K. A. Fischer, T. Sarmiento, K. G. Lagoudakis, Y. A. Kelaita, C. S. Muñoz, E. del Valle, F. P. Laussy, and J. Vučković, *Physical review letters* **114**, 233601 (2015).

[7] C. P. Dietrich, A. Fiore, M. G. Thompson, M. Kamp, and S. Höfling, *Laser & Photonics Reviews* (2016).

[8] A. Majumdar, M. Bajcsy, D. Englund, and J. Vuckovic, *IEEE Journal of Selected Topics in Quantum Electronics* **18**, 1812 (2012).

[9] H. Kim, R. Bose, T. C. Shen, G. S. Solomon, and E. Waks, *Nature Photonics* **7**, 373 (2013).

[10] T. Volz, A. Reinhard, M. Winger, A. Badolato, K. J. Hennessy, E. L. Hu, and A. Imamoğlu, *Nature Photonics* **6**, 605 (2012).

[11] R. Thompson, G. Rempe, and H. Kimble, *Physical Review Letters* **68**, 1132 (1992).

[12] A. Neuzner, M. Körber, O. Morin, S. Ritter, and G. Rempe, *Nature Photonics* **10**, 303 (2016).

[13] T. Zhong, J. M. Kindem, J. Rochman, and A. Faraon, *arXiv preprint arXiv:1604.00143* (2016).

[14] B. Hausmann, B. Shields, Q. Quan, Y. Chu, N. De Leon, R. Evans, M. Burek, A. Zibrov, M. Markham, D. Twitchen, *et al.*, *Nano letters* **13**, 5791 (2013).

[15] M. Radulaski, Y.-K. Tzeng, J. L. Zhang, K. G. Lagoudakis, H. Ishiwata, C. Dory, K. Alasaad, G. Ferro, Z.-X. Shen, N. Melosh, *et al.*, *arXiv preprint arXiv:1610.03183* (2016).

[16] D. O. Bracher and E. L. Hu, *Nano letters* **15**, 6202 (2015).

[17] A. Sipahigil, R. Evans, D. Sukachev, M. Burek, J. Borregaard, M. Bhaskar, C. Nguyen, J. Pacheco, H. Atikian, C. Meuwly, *et al.*, *Science* **354**, 847 (2016).

[18] A. Sipahigil, K. D. Jahnke, L. J. Rogers, T. Teraji, J. Isoya, A. S. Zibrov, F. Jelezko, and M. D. Lukin, *Physical review letters* **113**, 113602 (2014).

[19] P. G. Baranov, A. P. Bundakova, A. A. Soltamova, S. B. Orlinskii, I. V. Borovsky, R. Zondervan, R. Verberk, and J. Schmidt, *Physical Review B* **83**, 125203 (2011).

[20] I. Diniz, S. Portolan, R. Ferreira, J. Gérard, P. Bertet, and A. Auffeves, *Physical Review A* **84**, 063810 (2011).

[21] T. Schröder, M. E. Trusheim, M. Walsh, L. Li, J. Zheng, M. Schukraft, J. L. Pacheco, R. M. Camacho, E. S. Bielejec, A. Sipahigil, *et al.*, *arXiv preprint arXiv:1610.09492* (2016).

[22] D. A. Steck, University of Oregon (2007).

[23] J. C. L. Carreño, E. Z. Casalengua, E. del Valle, and F. P. Laussy, *arXiv preprint arXiv:1610.06126* (2016).

[24] R. Houdré, R. Stanley, and M. Illegems, *Physical Review A* **53**, 2711 (1996).

[25] J. Fink, R. Bianchetti, M. Baur, M. Göppl, L. Steffen, S. Filipp, P. Leek, A. Blais, and A. Wallraff, *Physical review letters* **103**, 083601 (2009).

[26] M. Koch, C. Sames, M. Balbach, H. Chibani, A. Kubanek, K. Murr, T. Wilk, and G. Rempe, *Physical review letters* **107**, 023601 (2011).